Absolute cross sections with polarization effects in Ne*$(2p^5 3p)$+He collisions: A detailed comparison between theory and experiment

Cristian Bahrim
Laboratoire Aimé Cotton, bâtiment 505 Campus d'Orsay, 91405 Orsay Cedex, France
and Laser Department, Institute of Atomic Physics, INFLPR, 76900 Bucarest-Magurele, Romania

Hélène Kucal
Laboratoire de Spectroscopie Atomique, ISMRA, Université de Caen, boulevard du maréchal Juin, 14034 Caen, France

Françoise Masnou-Seeuws
Laboratoire Aimé Cotton, bâtiment 505 Campus d'Orsay, 91405 Orsay Cedex, France
(Received 21 October 1996; revised manuscript received 9 April 1997)

Quantal calculations are presented for intramultiplet mixing collisions of Ne*$(2p^5 3p)$ with He($^1S_0$) in the 60–1250 meV collision energy range. The coupled equations are solved in a diabatic representation where the coupling terms are obtained using the model potential calculations of Hennecart and Masnou-Seeuws [J. Phys. B **18**, 657 (1985)] for the interaction of the Ne* outer electron with the two cores and values fitted on the spectroscopic data of Dabrowski and Herzberg [Mol. Spectrosc. **73**, 183 (1978)] for the core-core interaction. An extensive comparison with the experimental data of the Eindhoven group is presented for absolute polarized cross sections and anisotropy parameters. Very good agreement is obtained with thermal energy data of Manders *et al.* [Phys. Rev. A **39**, 4467 (1989)], while the systematic 30–40 % discrepancy with superthermal data of Boom *et al.* [Phys. Rev. A **49**, 4660 (1994)] might be attributed to a calibration problem in the experiment rather than to an inaccuracy in the long-range potentials. [S1050-2947(97)09207-X]

PACS number(s): 34.50.−s, 34.20.−b, 31.50.+w

I. INTRODUCTION

During the last decade, a major achievement in the field of atom-atom (molecule) collisions and molecular dynamics has been made by experimental devices combining molecular beams and polarized laser techniques. Vector properties could then be analyzed for a variety of systems (for references, see the review paper [1]), giving deeper insight into the physical processes. Important work has been done by the Eindhoven group [2–4], which has focused on intramultiplet mixing collisions of Ne*$(2p^5 3p)$ atoms with ground-state He atoms. In their experiment, a beam of metastable Ne atoms was excited with a polarized laser into a combination of Zeeman sublevels $J_i M_i$ of a short-lived Ne*$(2p^5 3p; 2p_i)$ level, labeled $2p_i$ according to Paschen notation. By varying the polarization vector of the exciting light and by measuring the population of the other $(2p_f; J_f)$ fine-structure levels by fluorescence analysis, it is possible to determine the absolute cross section $\sigma_{2p_i; J_i M_i \to 2p_f; J_f}$ for the reaction

$$\mathrm{Ne}^*(2p_i; J_i M_i) + \mathrm{He}(^1S_0) \to \mathrm{Ne}^*(2p_f; J_f) + \mathrm{He}(^1S_0) + \Delta E_{if}. \quad (1)$$

A strong polarization dependence was observed [3,4], revealing differences by a factor up to 3.5 between some cross sections $\sigma_{2p_i; J_i M_i = 0 \to 2p_f; J_f}$ and $\sigma_{2p_i; J_i M_i = 1 \to 2p_f; J_f}$ measured in the 50–150 meV energy range. The unpolarized cross sections $\sigma_{2p_i; J_i \to 2p_f; J_f}$ were also measured. For an interpretation of these data, molecular potential curves computed by Hennecart and Masnou-Seeuws [5] in the framework of a model potential treatment have been used. Such calculations provide either a nondiagonal matrix for the electronic Hamiltonian, which describes the perturbation of an excited neon atom by a ground-state helium atom at the internuclear distance R (diabatic picture), or adiabatic curves obtained by diagonalization of the electronic Hamiltonian and adapted to the Hund's case c coupling scheme.

Excellent agreement was obtained between the measured absolute cross sections at thermal energies (TE's) [3,4,6] and quantal calculations [4] using the diabatic picture and considering a large number of channels coupled by the electronic Hamiltonian. In some cases, where rotational coupling can be neglected, the unpolarized cross sections $\sigma_{2p_i; J_i \to 2p_f; J_f}$ can also be computed with very good accuracy using simple quantum calculations [5,7,8] considering two adiabatic states in Hund's case c representation coupled by radial coupling. In such cases a semiclassical model, using simple probabilities predicted by the Landau-Zener model [6] or a more accurate exponential model [7], has been proved to give a correct interpretation of the observed results: In such a model, the population is transferred from one molecular state to the other in a region of internuclear distances localized near an avoided crossing between two adiabatic potential curves.

However, when new experiments were performed [9] at superthermal (SE) collision energy ($200 < E < 1250$ meV), a marked disagreement was observed between quantal calculations and experiment, the measured cross sections being smaller than the computed ones by a factor varying from 0.9 to 0.4. Moreover, the authors [10] showed that in the quantal calculations a large part of the cross section was due to a contribution from impact parameters much larger than the avoided crossing position, so that a large part of the popula-

tion transfer from one molecular state to another one did occur at long range, far from any avoided crossing. This result seemed to indicate a failure of the previous semiclassical treatment in the range of superthermal energies, and the authors concluded [9,10] by casting doubt on the validity of the long-range part of the potentials of Hennecart and Masnou-Seeuws. This conclusion looks surprising, as the inadequacy of long-range potentials should lead to stronger discrepancies at low energies.

The aim of the present paper is to reconsider the problem and to give a more exhaustive comparison between coupled-channel quantal calculations and experimental results. In Sec. II, we shall discuss the potentials that were determined in Ref. [5], hereafter referred to as paper I. The problem of the short-range potential was not addressed properly in the quoted work and will be reconsidered here. In Sec. III, we shall describe our quantum treatment. In Sec. IV, we shall present the results of our calculations, compare with experiment, and discuss the sensitivity of the calculated cross sections to the potentials. Section V is the conclusion.

Atomic units will be used except when otherwise stated.

II. POTENTIALS

In the model potential calculations of paper I, the quantity which is determined accurately is the energy of one electron in the field of a Ne^+ ion and a ground-state helium atom at a distance R. The model is valid provided R is large enough so that the clouds of the two cores may be considered as distinct. The energy of the HeNe* molecule is then obtained by adding the core-core interaction, which is known at large internuclear distances through multipole expansion. So there is a critical distance R_{critical} below which the model is questionable. Indeed, the three-body problem is separated into three two-body problems, with a polarization correction.

(i) The interaction between the outer electron and the open-shell Ne^+ core is represented by the parametric model of Feneuille *et al.* [11], with first-order perturbation treatment of the fine structure and of the nonspherical part of the bielectronic interaction. The energy terms in the $|LSM_LM_S\rangle$ representation are given in a parametric [12] form, and the atomic energy levels in the $|2p_iJ_iM_i\rangle$ intermediate-coupling scheme are obtained by diagonalization of the matrix of spin-orbit coupling; the quantum numbers L,S,J then correspond, respectively, to the total orbital and spin angular momentum of the electrons in the $2p^53p$ configuration, and to their sum, the total electronic angular momentum **J**. Both spin-orbit constants and parameters representing the bielectronic interaction were fitted to the neon experimental spectrum.

(ii) The interaction between the outer electron and the ground-state helium atom is represented by a model potential fitted on low-energy electron-helium scattering data as described by Valiron *et al.* [13].

(iii) The core-core interaction is represented by the long-range multiple expansion which displays a R^{-4} behavior.

(iv) A three-body term deals with the nonadditivity of the potentials when the polarization electric fields are not collinear.

This model can be generalized when the overlap of the two core clouds is limited to the long-range exponential part

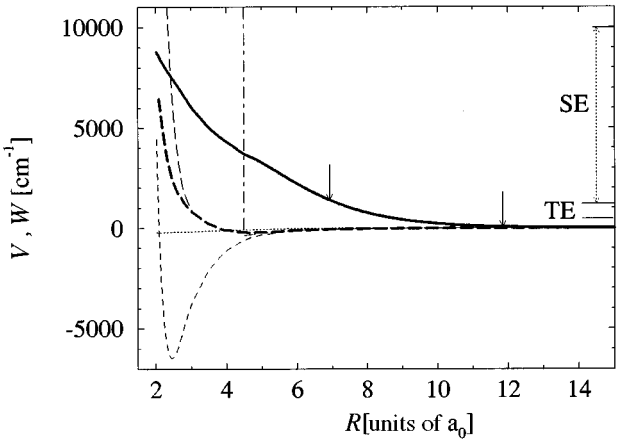

FIG. 1. Electrostatic potentials discussed in the present work for outer-electron- ($3p$-) core interaction, $\mathcal{V}_\sigma(R)$ (solid line) and $\mathcal{V}_\pi(R)$ (dotted line) [see Eq. (3) in text], and for core-core interaction, $\mathcal{W}_\sigma(R)$ (dashed line) and $\mathcal{W}_\pi(R)$ (long dashed line) [see Eq. (5) in text]. For $R<3a_0$ two potentials are presented: $\mathcal{W}_{\pi 1}(R)$ (thin long dashed line) and $\mathcal{W}_{\pi 2}(R)$ (thick long dashed line) corresponding to two arbitrary choices in the extrapolation of the $U_A(R)$ molecular potential of $HeNe^+$ ion for short internuclear distances. The core-core potential used in paper I for both symmetries is represented by a dash-dotted line (vertical wall and polarization potential). The vertical arrows indicate the distances where the difference $\mathcal{V}_\sigma(R)-\mathcal{V}_\pi(R)$ is equal to the maximum and minimum values of the fine-structure splitting between two neighboring levels. The energy range for SE and TE experiments is also indicated.

of the wave functions, according to the well-known asymptotic model [14,15]. This point, indicated in paper I, is developed further in the present work.

We shall consider a reference frame where the internuclear axis **R** is the quantization axis. In the formalism of paper I, the electronic Hamiltonian is written as a sum of effective operators:

$$\mathbf{H}_{\text{el}}(R,\mathbf{r})=\mathbf{H}_a(\mathbf{r})+\mathbf{V}_{\text{int}}(R)+\mathbf{W}_{\text{cc}}(R), \tag{2}$$

where $\mathbf{H}_a(\mathbf{r})$ is the atomic Hamiltonian of the neon atom, including fine structure, $\mathbf{V}_{\text{int}}(R)$ contains both the outer electron interaction with the perturber and the three-body term described in paper I, $\mathbf{W}_{\text{cc}}(R)$ is the Ne^+-He interaction, hereafter referred to as the core-core interaction, $\mathbf{r}$ is the positions vector for the $3p$ electron with respect to the center of mass of the nuclei, and R is the radial component of the internuclear vector **R**. For the sake of clarity, we note here that the atomic spin-orbit coupling of Ne* is not modified by the presence of He. The atomic Hamiltonian $\mathbf{H}_a(\mathbf{r})$ is diagonal in the $|2p_iJ\Omega\rangle$ representation, where Ω is the absolute value of the projection of **J** on the internuclear axis, the eigenvalues being the experimental energies of the various $2p_i$ states. The potential $\mathbf{V}_{\text{int}}(R)$ is a one-electron operator, and it is diagonal in the molecular basis $|3pl_e\lambda\rangle$, where λ is the projection of orbital angular momentum ($l_e=1$) of the outer electron on the quantization axis. We have drawn in Fig. 1 the quantities

$$\mathcal{V}_\sigma(R)=\langle 3p,l_e=1,\lambda=0|\mathbf{V}_{\text{int}}(R)|3p,l_e=1,\lambda=0\rangle, \tag{3}$$

$$\mathcal{V}_\pi(R)=\langle 3p,l_e=1,\lambda=\pm 1|\mathbf{V}_{\text{int}}(R)|3p,l_e=1,\lambda=\pm 1\rangle,$$

which were computed by Hennecart and Masnou-Seeuws up to $R=4.5a_0$ and simply extrapolated in the present paper in the region $2a_0<R<4.5a_0$, assuming an exponential behavior. The matrix elements of $\mathbf{V}_{\rm int}(R)$ in the $|2p_iJ\Omega\rangle$ representation have been given in Appendix 1 of paper I as a function of the quantities $\mathcal{V}_\sigma(R)$ and $\mathcal{V}_\pi(R)$. In the given reference there are two errors for $\Omega=1$ which must be corrected by

$$\langle 2,1,3,1|\mathbf{V}_{\rm int}(R)|2,1,3,1\rangle = +\frac{1}{15}[8\mathcal{V}_\sigma(R)+7\mathcal{V}_\pi(R)],$$

$$\langle 2,1,2,1|\mathbf{V}_{\rm int}(R)|1,1,1,1\rangle = -\frac{1}{4\sqrt{3}}[\mathcal{V}_\sigma(R)-\mathcal{V}_\pi(R)]. \quad (4)$$

The core-core interaction described by the effective operator $\mathbf{W}_{\rm cc}(R)$ has been defined in paper I by two matrix elements in the basis of $|L_cS_cM_LM_S\rangle$ states, which may be written, in the spirit of the asymptotic method [14,15], as

$$\mathcal{W}_\sigma(R)=\langle 2p^5;L_c=1M_L=0|\mathbf{W}_{\rm cc}(R)|2p^5;L_c=1M_L=0\rangle$$
$$=-\frac{\alpha_d}{2R^4}+W_\sigma^{\rm ex}(R),$$

$$\mathcal{W}_\pi(R)=\langle 2p^5L_c=1M_L=\pm1|\mathbf{W}_{\rm cc}(R)|2p^5L_c=1M_L=\pm1\rangle$$
$$=-\frac{\alpha_d}{2R^4}+W_\pi^{\rm ex}(R), \quad (5)$$

where α_d is the dipole polarizability of the He ground-state atom and was taken equal to 1.384 a.u. [16]; $W_\sigma^{\rm ex}(R)$ and $W_\pi^{\rm ex}(R)$ represent the exchange interactions between the electronic wave function of the Ne^+ ion in the $2p^5$ configuration and of the ground-state He atom. Equations (5) are valid provided that the overlap between the two electronic clouds is limited to the asymptotic region, where the wave functions display an exponential behavior corresponding to the classically forbidden region for the motion of the electrons [14,15]. The exponential behavior of $W_\sigma^{\rm ex}(R)$ and $W_\pi^{\rm ex}(R)$ is a check for the validity of our model.

In paper I, the exponential terms were only estimated following the theoretical work of Efremenkova *et al.* [17]. In the present work, we have chosen to determine $\mathcal{W}_\sigma(R)$ and $\mathcal{W}_\pi(R)$ from the adiabatic curves $U_X(R)$ and $U_A(R)$ that are deduced from molecular spectroscopy measurements of Dabrowski and Herzberg [18] concerning the $X\ ^2\Sigma_{1/2}$ and $A_2\ ^2\Pi_{1/2}$ states of the $HeNe^+$ molecular ion. The curves $U_X(R)$ and $U_A(R)$ are shown in Ref. [18]: As there are few bound states in the $U_A(R)$ potential, there is some uncertainty in the determination of the short-range part ($R<3a_0$) of the potential. The potential curves $\mathcal{W}_\sigma(R)$ and $\mathcal{W}_\pi(R)$ can easily be computed [19] as solutions of the following second-order equation:

$$\lambda^2-[U_X(R)+U_A(R)]\lambda+U_X(R)U_A(R)+\frac{C^2}{2}=0 \quad (6)$$

[$\lambda_1=\mathcal{W}_\sigma(R)$ and $\lambda_2=\mathcal{W}_\pi(R)+C/2$], where C is the spin-orbit coupling (which is assumed to be R independent and equal to the value $C=782\ {\rm cm}^{-1}$ of the ground-state Ne^+ ion). The energy origin is chosen at the center of gravity of the $Ne^+(2p^5)$ configuration. The core-core potentials $\mathcal{W}_\sigma(R)$ and $\mathcal{W}_\pi(R)$ are represented in Fig. 1. Due to the uncertainty of the $U_A(R)$ potential for $R<3a_0$, we present two potentials $\mathcal{W}_{\pi1}(R)$ and $\mathcal{W}_{\pi2}(R)$, which correspond to two choices for the short-range part of $U_A(R)$. The theoretical potential curves $U_X(R)$ and $U_A(R)$ of Efremenkova *et al.* [17] look more repulsive than those of Dabrowski and Herzberg [18]: For instance, the well in the $U_X(R)$ potential is very shallow and located at 4.3 instead of $2.45a_0$. Therefore, we had to reconsider in the present paper the core-core interaction used in the dynamical calculations of paper I, which was approximated by a repulsive wall located at $R=4.5a_0$, and by a polarization potential at larger distances as indicated in Fig. 1.

The exchange potentials $W_\sigma^{\rm ex}(R)$ and $W_\pi^{\rm ex}(R)$ can be deduced from $\mathcal{W}_\sigma(R)$ and $\mathcal{W}_\pi(R)$, respectively, by subtracting the polarization term [see Eq. (5)]. We have checked that for $R<R_{\rm critical}=3.5a_0$, such curves depart from the expected exponential behavior, making the model potential calculations for the He-Ne* system questionable.

Two main physical mechanisms can be considered in the collision problem. The first one, discussed in paper I, may be analyzed by comparing the splitting between the two curves $\mathcal{V}_\sigma(R)$ and $\mathcal{V}_\pi(R)$ to the order of magnitude of the fine-structure splitting between two neighboring $2p_i$ states, which varies between 59 and 1400 $\rm cm^{-1}$ for the transitions considered here, and to the collision energy (60–1250 meV, that is, 483–10 082 $\rm cm^{-1}$). Pseudocrossings in the adiabatic potential curves occur at distances where those two quantities have the same order of magnitude, as discussed in paper I and in Refs. [7,8]. The second mechanism is due to the rotation of the trajectory representing the relative motion of the nuclei and is mainly determined by the short-range potential, in particular by the position of the repulsive wall. We have indicated in Fig. 1 both the extreme values for the position of the pseudocrossings described above and the collision energy range. It is then manifested that calculations in the thermal energy range will not be very sensitive to the description of the core-core term, while the superthermal collisions will be controlled by the short-range potentials.

In Fig. 2, we compare the core-core potentials $\mathcal{W}_\sigma(R)$ and $\mathcal{W}_{\pi1}(R)$ used in the present work to the similar potentials $W_\sigma(R)$ and $W_\pi(R)$ proposed by Manders *et al.* [4] and used by the Eindhoven group in several papers [6,9,10]. The two sets of curves differ in the short-range part; besides, we find a different behavior in the region between $4a_0$ and $6a_0$ as $|\mathcal{W}_\sigma(R)|>|\mathcal{W}_\pi(R)|$, while the two curves $W_\sigma(R)$ and $W_\pi(R)$ cross. We justify our choice both by agreement with spectroscopy data and by physical arguments, the perturbation of a σ state being expected to be larger at long range. We shall therefore analyze the sensitivity of the cross sections to the choice of the core-core term and to the uncertainty of the model at short internuclear distances, in particular for the exact position of the repulsive wall.

In the dynamical treatment presented below, we solve the coupled equations in the framework of a diabatic representation in which the Hamiltonian $\mathbf{H}_a(\mathbf{r})$ is diagonal.

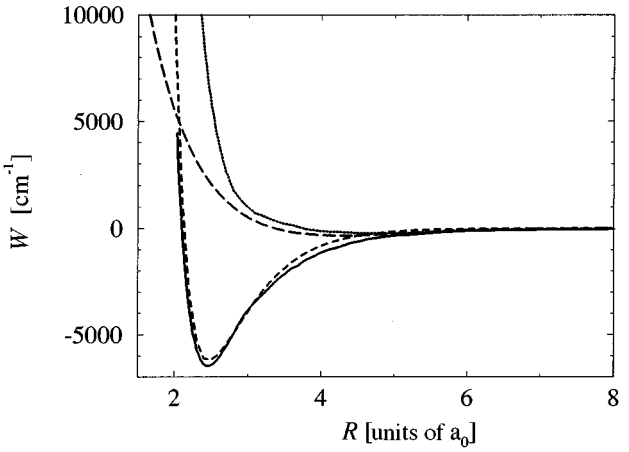

FIG. 2. Comparison between the core-core potentials $\mathcal{W}_\sigma(R)$ (solid line) and $\mathcal{W}_{\pi 1}(R)$ (dotted line) proposed in this paper and the similar potentials $W_\sigma(R)$ (dashed line) and $W_\pi(R)$ (long dashed line) proposed in Ref. [4] and used in several theoretical calculations by the Eindhoven group [4,6,9,10].

III. TREATMENT OF THE COLLISION PROBLEM

A. Coupled equations: Body-fixed and space-fixed representations

A full quantum-mechanical treatment of collision-induced fine-structure transitions has already been described in many papers [20–27], and for the Ne*$(2p^5 3p)$+He in Ref. [4]. We shall, however, present a coherent description of the formalism giving complementary information to previous work and adapted to lower-energy collisions where closed channels are present.

In the frame linked to the center of mass of the two colliding atoms, the total Hamiltonian may be written

$$\mathbf{H}(R,\theta,\varphi,\mathbf{r}) = -\frac{1}{2\mu}\left(\frac{\partial^2}{\partial R^2}+\frac{2}{R}\frac{\partial}{\partial R}\right)+\frac{\mathbf{N}^2(\theta,\varphi)}{2\mu R^2}+\mathbf{H}_{\rm el}(\mathbf{r},R), \tag{7}$$

where R, θ, φ are the spherical coordinates for the internuclear distance $\mathbf{R}$, μ is the reduced mass (6120 a.u.), and $\mathbf{N}^2$ the square of the angular momentum operator associated with the rotation of the internuclear axis. During the collision, this angular momentum is coupled with the total electronic momentum $\mathbf{J}$, giving the total momentum $\mathbf{P}=\mathbf{N}+\mathbf{J}$. The total wave function $\Psi(\mathbf{r},\mathbf{R})$ is expanded on a basis of functions which are built from eigenvectors of the operator $\mathbf{P}^2$, the projection $\mathbf{P}_z$ of $\mathbf{P}$ on the quantization axis, and the parity operator Π, with the eigenvalues $P(P+1)$, M_p, and π, respectively.

We have considered two frames: a body-fixed frame for which the quantization axis $\overrightarrow{Oz}$ is directed along the internuclear axis $\mathbf{R}$ and a space-fixed frame with a quantization axis $\overrightarrow{OZ}$ parallel to the initial asymptotic relative velocity $\mathbf{g}$. The space-fixed frame is linked to the body-fixed frame through a rotation by Euler angles (φ,θ,ω), where the first two angles are defined by the spherical coordinates (R,θ,φ) of the internuclear distance $\mathbf{R}$, in the space-fixed frame, while the third Euler angle ω is arbitrary.

In paper I the dynamical problem was solved using a two-state adiabatic expansion, computing the radial coupling matrix elements and neglecting the rotational coupling. One possibility to improve the accuracy of those calculations would be to include rotational coupling and use a larger number of adiabatic states in the expansion. We have chosen in the present work to use a diabatic representation by expanding the total wave function on the eigenstates of the atomic Hamiltonian $\mathbf{H}_a(\mathbf{r})$ and, therefore, considering the atom-atom interaction as a coupling term. The advantage of such representation is to avoid the cumbersome calculation of the radial and rotational coupling matrix elements. The drawback is that a larger number of coupled channels has to be considered.

We have expanded the total wave function $\Psi(\mathbf{r},\mathbf{R})$ considering the basis set defined by the complete operators set which commute with the total Hamiltonian. We shall note by the index γ the various molecular channels. In the body-fixed representation, the expansion on eigenfunctions of Π, $\mathbf{P}^2$, $\mathbf{P}_z$, $\mathbf{J}^2$, $\mathbf{J}_z$, and $\mathbf{H}_a(\mathbf{r})$ is

$$\Psi(\mathbf{r},\mathbf{R}) = \sum_P \sum_{M_p} \sum_\pi \sum_{2p_\gamma;J} \sum_\Omega \frac{1}{R} F^{\pi P M_P}_{2p_\gamma J\Omega}(R) \times |\pi P M_P;2p_\gamma J\Omega\rangle, \tag{8}$$

where

$$\begin{aligned}|\pi P M_P;2p_\gamma J\Omega\rangle &= \sqrt{\frac{1}{2-\delta_{\Omega,0}}}\left[\sqrt{\frac{2P+1}{8\pi^2}}D^{P*}_{M_P,\Omega}(\varphi,\theta,\omega)|2p_\gamma J\Omega\rangle\right.\\ &\pm(-1)^{P+J+L_c+l_e}(1-\delta_{\Omega,0})\sqrt{\frac{2P+1}{8\pi^2}}\\ &\left.\times D^{P*}_{M_P,-\Omega}(\varphi,\theta,\omega)|2p_\gamma J-\Omega\rangle\right].\end{aligned} \tag{9}$$

In Eq. (9), we have introduced the electronic states $|2p_\gamma J\Omega\rangle$, which are the eigenfunctions of the $\mathbf{J}^2$, $\mathbf{J}_z$, and $\mathbf{H}_a(\mathbf{r})$ operators and the normalized symmetric top functions $[\sqrt{(2P+1)/8\pi^2}]D^{P*}_{M_P,\Omega}(\varphi,\theta,\omega)$, defined following the conventions of Ref. [28], which are the eigenfunctions of the $\mathbf{P}^2$ and $\mathbf{P}_z$ operators. It can be shown that in this frame the parity of the state is $\pi=\pm(-1)^{P+J+L_c+l_e}$, and it reduces to $\pm(-1)^{P+J}$ for the $2p^5 3p$ configuration of the Ne* atom (because $L_c=l_e=1$). The notation π for the parity should not be confused with the number π which appears in the equations.

For the sake of simplicity, in the following we shall use the notation α for the $2p_\gamma,J,\Omega$ indexes of a given channel, so that the radial wave function will be written $F^{\pi F M_P}_\alpha(R)$. For an ingoing molecular channel α, we have to solve a set of coupled differential equations

$$\frac{d^2F_\alpha^{\pi PM_P}(R)}{dR^2}+\left(k_\gamma^2-\frac{P(P+1)+J(J+1)-2\Omega^2}{R^2}\right)\times F_\alpha^{\pi PM_P}(R)$$
$$=\sum_{\alpha'}2\mu\left[\langle\alpha'|\mathbf{V}_{\rm int}(R)+\mathbf{W}_{\rm cc}(R)|\alpha\rangle-\frac{1}{2\mu R^2}\langle\alpha'|P_+J_-+P_-J_+|\alpha\rangle\right]F_{\alpha'}^{\pi PM_P}(R), \quad (10)$$

where $k_\gamma^2=2\mu[E-E(2p_\gamma)]$, for different values of parity $\pi=\pm(-1)^P$ and P quantum numbers, M_P being arbitrary. The diabatic electronic coupling term $\langle\alpha'|\mathbf{V}_{\rm int}(R)+\mathbf{W}_{\rm cc}(R)|\alpha\rangle$ in Eq. (10), can be easily obtained from formulas (3) and (5). The second coupling term in Eq. (10) is the rotational coupling.

We have checked the possibility of excluding some of the 23 different molecular channels in the expansion. It is justified in the present range of energies to exclude the remote $2p_1$ channel, which corresponds to $J=0$: For example, if $2p_5$ is the initial level, the $2p_1$ channel opens at collision energies above 272 meV, and from 0.280 until 1 eV the relative variation of the unpolarized or polarized cross sections is less than 1% when this channel is included. Above 1 eV, the relative variation is less than 2%. In contrast, although the $2p_{10}$ level also lies far from the nearest level $(2p_9)$ (the gap being $\Delta E_{9,10}=1399.41\ {\rm cm}^{-1}$), the contribution of the three molecular channels correlated to this dissociation limit cannot be neglected and they are included in our calculations. Therefore, we have solved two sets of 17 and 18 differential coupled equations set in subspaces defined by $\pi=+(-1)^P$ and $\pi=-(-1)^P$ parity, respectively.

Alternatively, in the space-fixed representation we have expanded the total wave function $\Psi(\mathbf{r},\mathbf{R})$ on eigenfunctions of Π, $\mathbf{N}^2$, $\mathbf{N}_Z$, $\mathbf{J}^2$, $\mathbf{J}_Z$, and $\mathbf{H}_a(\mathbf{r})$ operators, where $\mathbf{J}_Z$ means the projection of $\mathbf{J}$ on the $\overrightarrow{OZ}$ quantization axis:

$$\Psi(\mathbf{r},\mathbf{R})=\sum_P\sum_{M_p}\sum_\pi\sum_{2p_\gamma;J}\sum_N\frac{1}{R}G_{2p_\gamma JN}^{\pi PM_P}(R)\times|\pi PM_P;2p_\gamma JN\rangle, \quad (11)$$

where

$$|\pi PM_P;2p_\gamma JN\rangle=\sum_M\sum_{M_N}(-1)^{-J+N-M_P}\sqrt{2P+1}\begin{pmatrix}J & N & P\\ M & M_N & -M_P\end{pmatrix}\times Y_{M_N}^N(\theta,\varphi)|2p_\gamma JM\rangle. \quad (12)$$

The atomic eigenfunctions $|2p_\gamma J\Omega\rangle$ (body-fixed frame) can be expressed as a linear combination of the atomic eigenfunctions $|2p_\gamma JM\rangle$ (space-fixed frame). In Eq. (12), $\left(\begin{smallmatrix}J & N & P\\ M & M_N & -M_P\end{smallmatrix}\right)$ is a $3j$ symbol. As above, we shall simplify the notation by calling β the $2p_\gamma,J,N$ channel, so that the radial wave functions are written $G_\beta^{\pi PM_P}(R)$ for various space-fixed channels. It is a simple fact to show that the eigenvalue of parity operator, in the space-fixed representation, is $\pi=(-1)^{N+L_c+l_e}$, which reduces to $(-1)^N$ for the $2p^53p$ configuration. We note that for each $2p_\gamma J$ atomic level and for a given P, the quantum number N may take $2J+1$ values, hereafter written N_β. The coupled equations are then written for an ingoing molecular channel β, in each subspace defined by π, P, and M_P quantum numbers, as

$$\frac{d^2G_\beta^{\pi PM_P}(R)}{dR^2}+\left(k_\gamma^2-\frac{N_\beta(N_\beta+1)}{R^2}\right)G_\beta^{\pi PM_P}(R)=\sum_{\beta'}2\mu\langle\beta'|\mathbf{V}_{\rm int}(R)+\mathbf{W}_{\rm cc}(R)|\beta\rangle G_{\beta'}^{\pi PM_P}(R). \quad (13)$$

It is possible to switch from one representation to the other via the unitary transformation

$$|\pi PM_P;\beta\rangle=\sum_\beta W_{\beta;\alpha}^{\pi PM_P}|\pi PM_P;\alpha\rangle, \quad (14)$$

where

$$W_{\beta;\alpha}^{\pi PM_P}=\sqrt{\frac{2}{1-\delta_{\Omega,0}}}\sqrt{2N_\beta+1}(-1)^{N_\beta-J-\Omega}\times\begin{pmatrix}J & N_\beta & P\\ \Omega & 0 & -\Omega\end{pmatrix}. \quad (15)$$

We note that $W_{\beta;\alpha}^{\pi PM_P}$ is a block diagonal matrix which has nonvanishing nondiagonal elements only for the set of molecular channels which are correlated to the same $2p_iJ_i$ fine-structure atomic level. As the matrix elements of $\mathbf{V}_{\rm int}(R)$ and $\mathbf{W}_{\rm cc}(R)$ are readily obtained in the body-fixed representation, Eq. (13) involves transformation of the diabatic coupling matrix elements through Eq. (14) at *each* integration step. So it is not surprising that the calculations in the space-fixed representation are time consuming.

In order to extract the **S** matrix, the coupled equations (10) and (13) should be integrated up to a distance $R_{\rm max}$, where all coupling terms vanish and the adiabatic potentials are constant, so that the radial functions $F_\alpha^{\pi PM_P}(R)$ or $G_\beta^{\pi PM_P}(R)$ can be identified with known analytic solutions of the scattering problem with zero interaction. Because of the very slow decrease of the rotational coupling at large internuclear distances, the $R_{\rm max}$ value in the calculations using a body-fixed representation is found much larger than when the space-fixed representation is used. Therefore, in the present work, we have solved the coupled-channel equations (10) up to a particular distance $R_{\rm max}$, where we have switched representation using the unitary transformation (14) and considered the solutions of the coupled equations set (13) in a space-fixed frame. The $R_{\rm max}$ value was chosen after the analysis of the scattering **S**-matrix convergence. This aspect will be discussed later.

The change of representation implies that the radial wave functions $G_\beta^{\pi PM_P}(R)$ are expressed as a linear combination of the body-fixed radial solutions $F_\alpha^{\pi PM_P}(R)$. Therefore, for a given value of P, we have several asymptotic functions corresponding to the various N_β values. This can be readily seen from Eq. (13), where the centrifugal term $N_\beta(N_\beta+1)/R^2$ depends upon the particular β channel, in contrast to Eq. (10), where $P(P+1)/R^2$ is the same for *all* α chan-

nels of a given P. The radial wave functions $G_\beta^{\pi P M_P}$, for any β exit channel, must respect the usual boundary conditions:

$$G_\beta^{\pi P M_P}(R \equiv R_{\min}) = 0, \tag{16}$$

$$G_\beta^{\pi P M_P}(R \equiv R_{\max}) = J_{N_\beta}(k_\gamma R_{\max}) + K_{\beta;\beta'}^{\pi P M_P}(R_{\max}) \times N_{N_{\beta'}}(k_{\gamma'} R_{\max}), \tag{17}$$

where $K_{\beta;\beta'}^{\pi P M_P}$ are the elements of the scattering **K** matrix, while the functions J_{N_β} and N_{N_β} are the Ricatti-Bessel functions regular and irregular at the origin ($R_{\min}$) for open channels $k_\gamma^2 \geqslant 0$ or modified spherical Bessel functions of the first and third kinds, respectively, for closed channels. The scattering **S** matrix is then defined in the usual way from the open-open block of the scattering **K** matrix:

$$\mathbf{S} = \frac{\mathbf{I} + i\mathbf{K}_{oo}}{\mathbf{I} - i\mathbf{K}_{oo}}, \tag{18}$$

where **I** is the unitary matrix.

The polarized cross section is obtained from the **S** matrix after some algebra. It is a simple fact to express the scattering amplitudes in the space-fixed representation [15] from the boundary conditions of the total wave function of the system in a subspace defined by π, P, and M_P quantum numbers:

$$f_{2p_i;J_iM_i \to 2p_f;J_fM_f}(\mathbf{k}_i, \mathbf{k}_f) = \frac{2\pi i}{\sqrt{k_i k_f}} \sum_{P=P_{\min}}^{P_{\max}} \sum_{M_P=-P}^{P} \sum_{N=|P-J_i|}^{P+J_i} \sum_{N'=|P-J_f|}^{P+J_f} \sum_{M_N=-N}^{N} \sum_{M'_N=-N'}^{N'} i^{N-N'}(-1)^{-(N+N')}(2P+1) Y_{M_N}^N(\hat{k}_i) Y_{M'_N}^N(\hat{k}_f) \times (\delta_{J_jJ_i}\delta_{N'N} - S^P_{J_fN';J_iN}) \begin{pmatrix} N & J_i & P \\ M_N & M_i & -M_P \end{pmatrix} \begin{pmatrix} N' & J_f & P \\ M'_N & M_f & -M_P \end{pmatrix}. \tag{19}$$

As J can reach the value 3 and as $J-N \leqslant P \leqslant J+N$, the minimum value of N being 0, $P_{\min}$ is equal to 3. Because of the choice of a space-fixed frame with the quantization axis along the asymptotic incident relative impulsion $\mathbf{k}_i$ [its polar angles being $\hat{k}_i = (0,0)$], the scattering amplitude formula has a more simple form. A supplementary simplification can be done considering that the nuclear rotation momentum is perpendicular to the asymptotic relative impulsion $\mathbf{k}_i$, and in consequence, we have $M_N = 0$ and $M_P = M_i$. Considering these simplifications in the formula (19) of the scattering diffusion amplitude and integrating the absolute value of it on all diffusion angles $\mathbf{k}_f$, we can readily obtain the cross section for transition between Zeeman sublevels and the polarized cross sections $\sigma_{2p_i;J_iM_i \to 2p_f;J_f}$ necessary to interpret the experiments of the Eindhoven group are readily obtained as

$$\sigma_{2p_i,J_iM_i \to 2p_f;J_f} = \frac{\pi}{k_i^2} \sum_{P=P_{\min}}^{P_{\max}} \sum_{N=|P-J_i|}^{P+J_i} \sum_{N''=|P-J_i|}^{P+J_i} \sum_{N'=|P-J_f|}^{P+J_f} i^{N-N''} \sqrt{(2N+1)(2N''+1)}(-1)^{-N-N''}(2P+1) \begin{pmatrix} N & J_i & P \\ 0 & M_i & -M_i \end{pmatrix} \times \begin{pmatrix} N'' & J_i & P \\ 0 & M_i & -M_i \end{pmatrix} (\delta_{J_fJ_i}\delta_{N'N} - S^P_{J_fN';J_iN})(\delta_{J_fJ_i}\delta_{N'N''} - S^P_{J_fN';J_iN''})^*$$

$$= \sum_{P=P_{\min}}^{P_{\max}} \sigma^P_{2p_i;J_iM_i \to 2p_f;J_f}, \tag{20}$$

where $\sigma^P_{2p_i;J_iM_i \to 2p_f;J_f}$ means the partial polarized cross section. Next, the unpolarized cross section for fine-structure transitions is

$$\sigma_{2p_i;J_i \to 2p_f;J_f} = \frac{\pi}{k_i^2} \sum_{P=P_{\min}}^{P_{\max}} \frac{(2P+1)}{(2J_i+1)} \sum_{N=|P-J_i|}^{P+J_i} \sum_{N'=|p-J_f|}^{P+J_f} |\delta_{J_fJ_i}\delta_{N'N} - S^P_{J_fN';J_iN}|^2. \tag{21}$$

It is worthwhile to note that the unpolarized inelastic cross section $\sigma_{2p_i;J_i\rightarrow 2p_f;J_f}$ depends only upon the absolute value of the **S**-matrix elements, while the polarized cross sections (20) contain interference terms. In the formulas (20) and (21), $P_{\min}$ is equal to 3 (see above), while the value of $P_{\max}$ is established through a convergence test.

B. Numerical treatment and convergence of the calculations

In the present work only open channels have been considered. We have solved the coupled differential equations (10) in the body-fixed representation, using a Johnson algorithm with constant step size [29,30], which provides a numerical determination of the logarithmic derivative of the radial function. Because of the very strong repulsive character of the electronic potentials at short distances, we have checked that the starting point of the integration could be $R_{\min}=2a_0$. The integration step size was chosen so that for each logarithmic derivative function, at least ten values of R were computed for half of an oscillation. The maximum value of the asymptotic wave number was estimated by considering the difference between the collision energy and the splitting between the ingoing channel and the lowest possible exit channel, which in our case is the $2p_{10}$ channel. This leads to a typical step size varying from $0.03a_0$ at a collision energy $E=0.1$ meV to $0.014a_0$ at $E=1$ eV. As we shall discuss below, the integration up to $R_{\max}=20a_0$ was found to be sufficient, so that the typical number of integration steps was varying from 600 at $E=100$ meV until 1300 at $E=1$ eV. At this distance, we have changed representation by an appropriate transformation derived from Eq. (14).

At $R_{\max}$, in the space-fixed representation, the different radial equations become completely uncoupled and we have evaluated the scattering **K** matrix and deduced the **S** matrix through formula (18). The convergence of the integration can then be checked from the stability of the **S**-matrix elements relative to the choice of $R_{\max}$.

In the body-fixed representation, the coupled equations (10) involve a diabatic electronic coupling term, which vanishes at $R\sim 15a_0$, and a rotational coupling one, which leads to population transfer between the various Zeeman sublevels of a given $2p_\gamma$ manifold and vanishes slowly. Our analysis has shown that, in order to compute the unpolarized cross section $\sigma_{2p_i;J_i\rightarrow 2p_f;J_f}$, it is sufficient to perform the numerical integration up to a distance $R=R_{\max}\sim 15a_0$. In contrast, because of the very slow variation of the rotational coupling term, in order to obtain accurate results for the polarization cross sections $\sigma_{2p_i;J_iM_i\rightarrow 2p_f;J_f}$ we should perform integration of the coupled equations (10) up to a larger internuclear distance (for example, at $E=100$ meV, $R_{\max}$ must be up to $1000a_0$).

The frame transformation (14) allows us to switch to the space-fixed representation, where the rotational coupling vanishes. However, as was discussed in the previous section, the radial function for a partial wave P corresponds to various partial waves N, from $|P-J|$ to $P+J$, each one having to be compared with a Ricatti-Bessel function of different order N, therefore having a different phase. One could be tempted to neglect this difference of phase because of the small value of the quantum number $J\leqslant 3$ compared to P: In the collision energy range considered here, the cross section is dominated by the contribution of the partial waves with $P\gg 10$, suggesting the assumption $N\sim P$. This approximation is valid provided that we can neglect the small variations of the phase of the **S**-matrix elements when the partial wave number is varying by a few units. It would be very convenient for treatment of the collisions in presence of a magnetic field.

We have checked this approximation at various collision energies, and we discuss here, as an example, the case of the $2p_5\rightarrow 2p_7$ transition at $E=100$ meV collision energy, where a strong polarization effect was observed (see Ref. [3]). If we characterize the polarization effect by the ratio $\sigma_{2p_5;M_i=0\rightarrow 2p_7}/\sigma_{2p_5;M_i=1\rightarrow 2p_7}$, for $R_{\max}=15a_0$ we obtain $\rho=0.3$, with the assumption $N\sim P$, and $\rho=3.7$ when the cross sections are calculated after the frame transformation using the correct value of N for each channel. This latter value is in good agreement with the experimental result $\rho=3.5$. However, the unpolarized cross section obtained in the approximation $N\sim P$, is $3.68\times 10^{-16}\ cm^2$, like in ''exact'' calculations, and the value $R_{\max}=15a_0$ is then sufficient.

In Fig. 3, we have represented the phase of a relevant matrix element $S_{J_i=1,N=1;J_f=1N'=1}$ as a function of the partial wave N, for various choices of $R_{\max}$. We can see that for calculations using the approximation $N\sim P$ [see Fig. 3(b)] the phase is not converging even when the integration is performed up to very large $R_{\max}$ values. In contrast, for exact calculations the convergence of the **S**-matrix element phase is already obtained for $R_{\max}=20a_0$ [see Fig. 3(a)]. The physical explanation of this effect relies upon the large value of the classical scattering angle: Because of the large value of its derivative, the phase is a rapidly varying function of N. When higher collision energies are considered, this effect decreases and the approximation $N\sim P$ starts to be valid [32].

As a conclusion, we may say that the polarized cross sections are highly sensitive to the accuracy of the procedure of phase extraction. This conclusion is important for further work considering collisions in the presence of a magnetic field.

IV. RESULTS AND DISCUSSION

In the present paragraph, we shall first discuss how the present calculations compare with the experimental data and with the previous calculations. Then we shall discuss the sensitivity of our calculations to the choice of the potentials.

A. Calculated cross sections: Comparison with experiment

We have calculated the unpolarized cross sections $\sigma_{2p_i;J_i\rightarrow 2p_f;J_f}$ and the polarized cross sections $\sigma_{2p_i;J_iM_i\rightarrow 2p_f;J_f}$ for all the transitions in which the initial states are $2p_2$ to $2p_{10}$, for collision energies varying from 60 to 1250 meV, in the range where experimental results are available (see Manders *et al.* [3,4,31] and Boom *et al.* [9,10]).

The experimental apparatus used by Manders *et al.* and by Boom *et al.* was carefully designed for measurements of absolute cross sections. Two atomic beams (a metastable neon beam and a ground-state helium beam) and a polarized

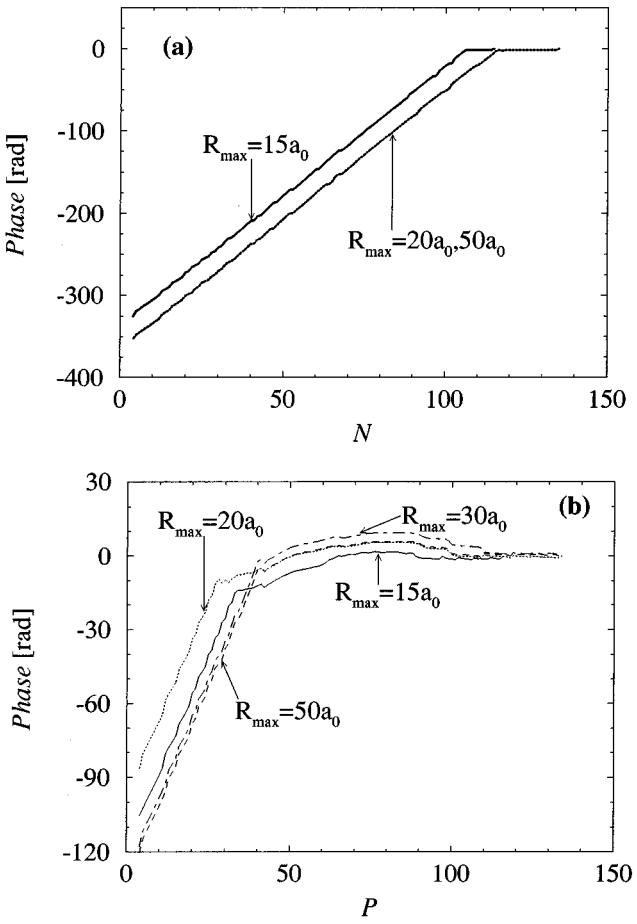

FIG. 3. (a) Phase of the **S**-matrix element $S_{J_i=1,N=1\rightarrow J_f=1,N'=1}$ in space-fixed representation, for the $2p_5\rightarrow 2p_7$ transition, at $E=100$ meV, as a function of the partial wave number N; the results were obtained by numerical integration of the coupled-channel equations (10) up to $R_{\max}=15a_0$, $20a_0$, and $50a_0$ and after the switch of representation. The two last lines cannot be differentiated. (b) Same as (a), when the integration of coupled equations (10) is performed up to $R_{\max}=15a_0$ (solid line), $20a_0$ (dotted line), $30a_0$ (dot-dashed line), and $50a_0$ (dashed line), assuming $N\sim P$ in the frame transformation.

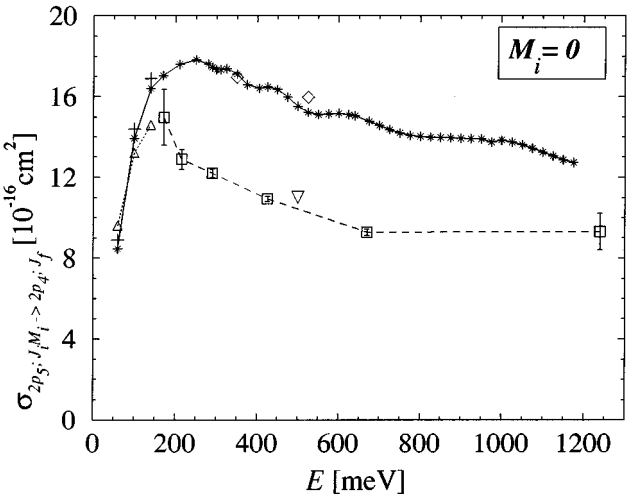

FIG. 4. Polarized cross sections $\sigma_{2p_5;J_iM_i=0\rightarrow 2p_4;J_f}$ as a function of the collision energy E: asterisks, present calculations; up triangles, TE experimental results [4,6]; squares, SE experimental results [9]; down triangle, non-energy-resolved experimental result [10]; crosses, previous TE quantal calculations [4,6]; and diamonds, SE quantal calculations [10]. The error bars represent the statistical error only, for SE experimental data; in the case when an error bar is less than the size of the square, we have chosen it to be equal with this size. The lines are drawn only as a guide to the eye.

laser beam cross at right angles. Once a metastable neon atom is excited by the laser into a $\{2p^5 3p;2p_iJ_i\}$ short-lived Ne* state, it may undergo an inelastic collision with a helium atom. The populations of the initial $2p_iJ_i$ and final $2p_fJ_f$ levels were determined by photodetection of the fluorescence light of the $2p_i\rightarrow 1s_l$ and $2p_f\rightarrow 1s_k$ transitions, respectively. Two sets of experiments have been performed. The main difference between them is the nature and energy of the primary neon metastable beam source.

In the first set of experiments [3,4,6,31], hereafter referred to as TE experiments, the primary beam originated in a discharge-excited supersonic expansion or a thermal metastable source. The TE collision energies varied from 60 to 150 meV. In the second set [9,10], hereafter referred to as SE experiments, a hollow cathode arc was used as a source and located at larger distance from the scattering center. The collision energies available with this source varied from 170 to 1250 meV (superthermal collision energy range). Two different detection methods were used in the SE experiments [9]: the pseudorandom correlation time-of-flight method, hereafter noted RC, and the single-burst time-of-flight method, hereafter referred to as SB.

The excellent performance of both sources allowed the experimentalists in Eindhoven to measure the *absolute* unpolarized and polarized cross sections for the various intramultiplet transitions in the neon $2p^5 3p$ configuration, with a very good accuracy. An important discussion concerns the sources of error. In Ref. [9], Tables V and VI, the authors have published absolute cross sections, with a few percent statistical errors indicated by error bars. The other experimental data are published without those statistical errors. Moreover, systematic errors are also discussed, which depend upon the geometry of the experiment (incident flux) and upon the calibration of the detection procedure. In the TE experiments, the systematic error is estimated to be 14% [4,10]; in SE experiments, as the source is located at larger distance, the authors indicate the possibility of a 22% systematic error [10]. We shall therefore discuss the comparison between our calculations and the experiment by considering both absolute cross sections and relative quantities such as the ratio of two cross sections.

It is hardly possible to present all calculated cross sections, and so we shall limit ourselves to a few examples: We will focus our attention on a few transitions for which experimental results are available.

We illustrate in the Figs. 4–8, the comparison between our calculations and the TE or SE experimental results or previous quantal calculations of the Eindhoven group [4,6,9,10]. We show the energy variation of our computed cross sections in the 60–1250 meV energy range for several transitions:

$$2p_5;J_i=1,M_i\rightarrow 2p_f;J_f$$

(with $M_i=0,1$ and $f=4,6,7,9$),

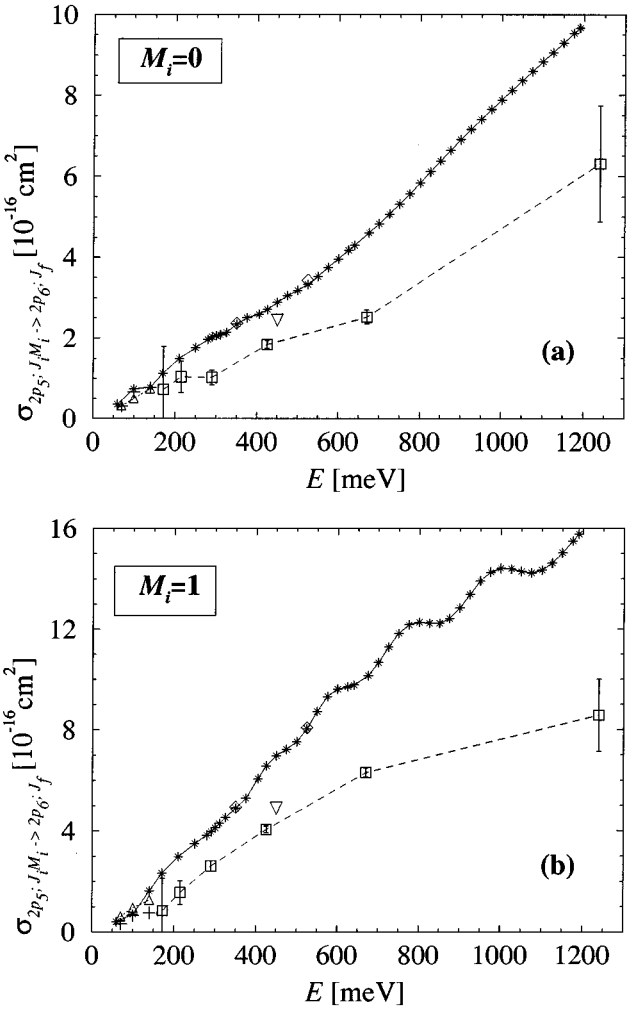

FIG. 5. Same as Fig. 4 for the variation of the polarized cross sections $\sigma_{2p_5;J_iM_i\to 2p_6;J_f}$ as a function of the collision energy E, with (a) $M_i=0$ and (b) $M_i=1$.

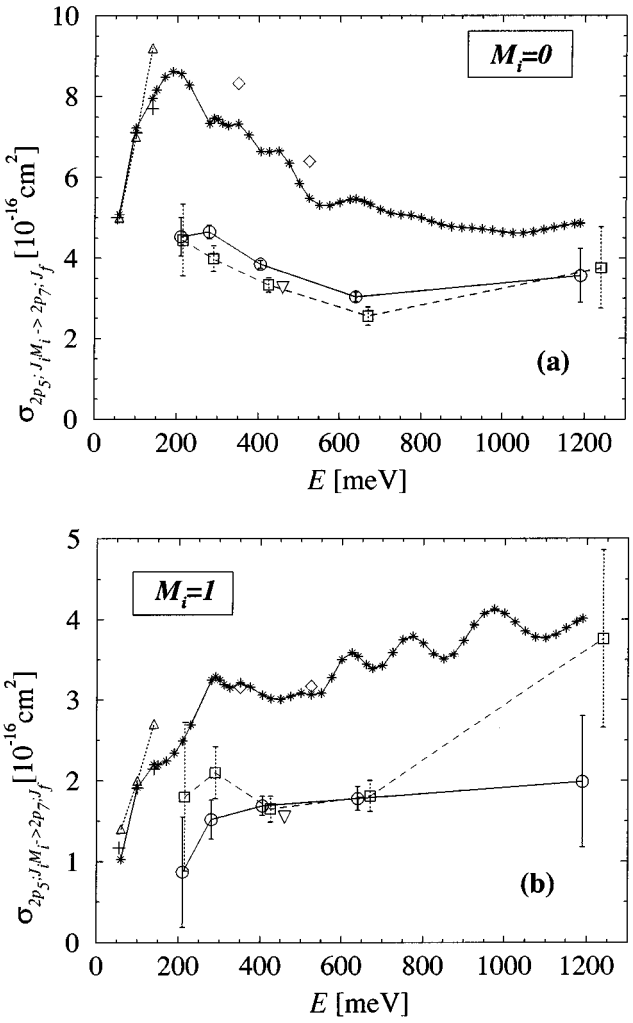

FIG. 6. Polarized cross sections $\sigma_{2p_5;J_iM_i\to 2p_7;J_f}$ as a function of the collision energy E. (a) corresponds to $M_i=0$; (b) corresponds to $M_i=1$. Same conventions as for Fig. 4, square symbols being for the single-burst (SB) type of SE experiments and circle symbols for the pseudorandom correlation (RC) type of SE experiments, according to Ref. [9].

and

$$2p_7;J_i=1,M_i\to 2p_6;J_f \quad (\text{with } M_i=0,1).$$

The analysis of Figs. 4–8 shows a very good agreement between our calculations and the TE experiments. This agreement was already found at a few energy values by Manders *et al.* [6], and we confirm their conclusion concerning the accuracy of the potential curves.

In contrast, for $E>170$ meV a large discrepancy (up to a factor of 2) exists between our calculations and SE experimental results. The small differences between our results and the few computed values published by Boom *et al.* [10] can be attributed to the difference in the choice of the core-core interaction, shown above in Fig. 2. The present calculations confirm the earlier conclusion of the Eindhoven group concerning the problem in the comparison between theory and SE experiments. As already mentioned in the Introduction, the authors have attributed this discrepancy to errors in the long-range potential. However, it is clearly manifested in the Figs. 4–8 that the experimental and theoretical polarized cross sections exhibit a very similar energy variation. We therefore propose to consider also the possibility of a calibration systematic error in the SE experiments much larger than the 22% factor given by the authors (see Ref. [10]). One possible check of such a hypothesis could be the presence of a discontinuity between the two sets of the experiment. Such a discontinuity is not manifested clearly in most cases: Within the statistical error bars, it is possible to make a continuous link between TE and SE experimental results. However, for the $2p_5\to 2p_7$ transition, which is a test transition [2,3,4,31], a discontinuity of a factor of 2 does exist [see Figs. 6(a) and 6(b)], which favors our hypothesis. It should be noted that this is the only case where the cross section is not abruptly rising in the region where the two sets of experiments overlap. In the other cases, the continuous link could also be explained by a small difference in the energy definition within two sets of experiments.

In Figs. 4–8, an oscillatory behavior in the energy variation of the calculated polarized cross sections, more obvious in SE range, is manifested. Unfortunately, because of the limited number of experimental points, this interference ef-

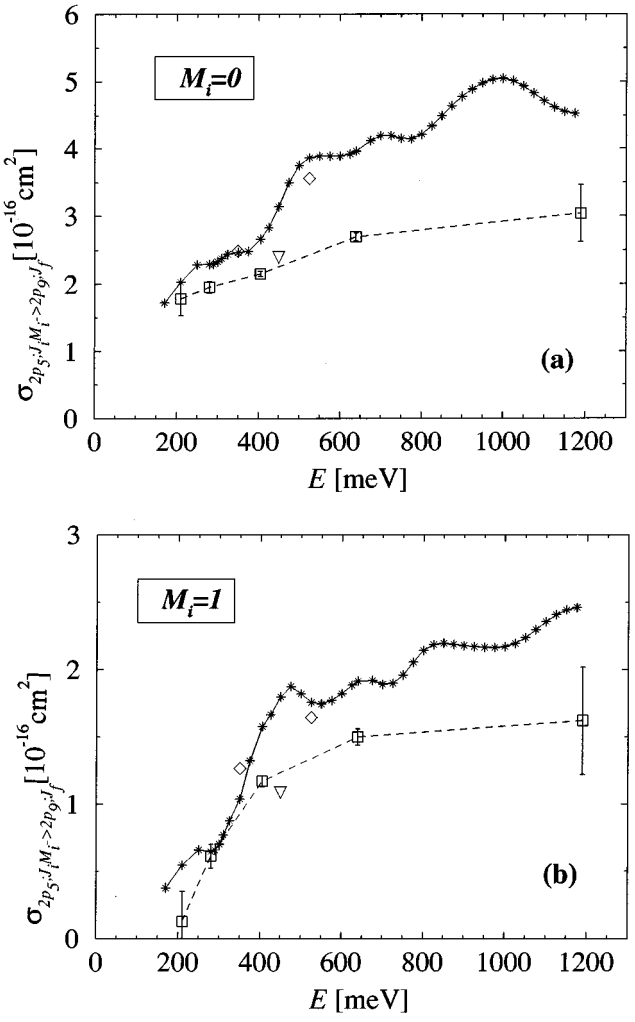

FIG. 7. Same as Fig. 4 for the variation of the polarized cross sections $\sigma_{2p_5;J_iM_i\to 2p_9;J_f}$ as a function of the collision energy, with (a) $M_i=0$ and (b) $M_i=1$.

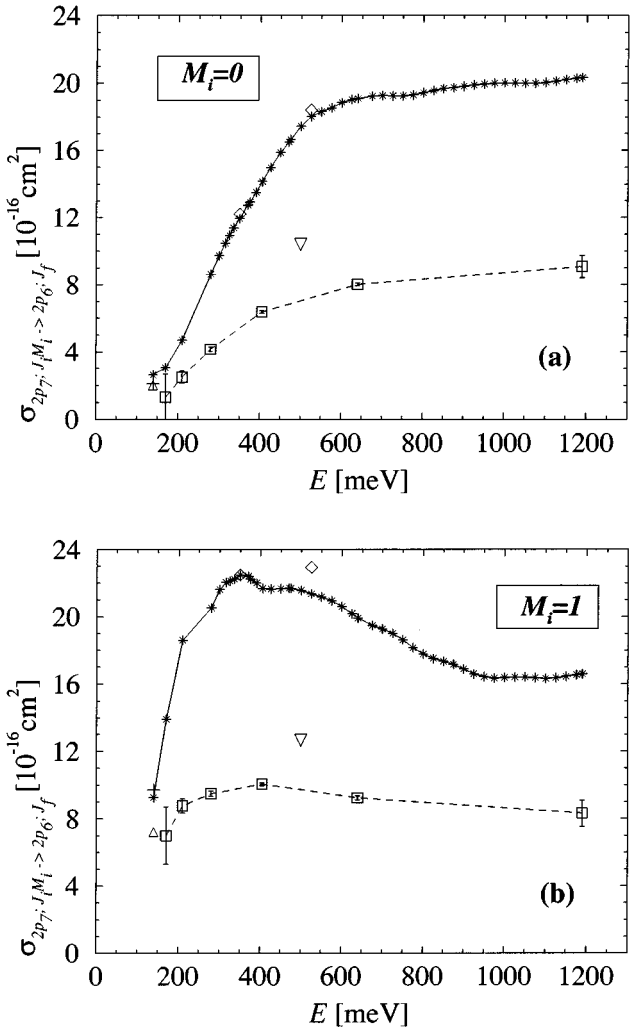

FIG. 8. Same as Fig. 4 for the variation of the polarized cross-sections $\sigma_{2p_7;J_iM_i\to 2p_6;J_f}$ as a function of the collision energy E, with (a) $M_i=0$ and (b) $M_i=1$.

fect, discussed in more detail in Ref. [32], cannot be confirmed by experiment. The resonant structure of the energy variation of the cross section was already shown in several recent papers (see, for example, Refs. [7,8,23]).

A more direct check of the experiments is the so-called ''β dependence'' of the cross sections, because the absolute polarized cross sections $\sigma_{2p_i;J_iM_i\to 2p_f;J_f}$ were determined by varying the β angle between the direction of electric field vector **E** of the linearly polarized laser light (the optical quantization axis in the photon frame) and the relative asymptotic velocity **g**. In general, the observed absolute cross section is found to be an incoherent sum over the Zeeman initial M_i sublevels:

$$\sigma^{(E)}_{2p_i;J_i\to 2p_f;J_f}(\beta)=\sum_{m_i} g_{m_i}\sum_{M_i}[d^{J_i}_{m_iM_i}(\beta)]^2\sigma_{2p_i;J_iM_i\to 2p_f;J_f}, \tag{22}$$

where $d^{J_i}_{m_iM_i}(\beta)$ are the reduced Wigner rotation functions and g_{m_i} is the relative population of Zeeman sublevels m_i, in the photon frame. When a linearly polarized laser light is used and in the cases where the initial levels are $|2p_i;J_i=1,M_i\rangle$, Eq. (22) becomes

$$\begin{aligned}\sigma^{(E)}_{2p_i;J_i=1\to 2p_f;J_f}(\beta)&=\frac{1}{2}\left(\sigma_{2p_i;J_i=1,M_i=0\to J_f}+\sigma_{2p_i;J_i=1,M_i=1\to J_f}\right)\\&+\frac{1}{2}\left(\sigma_{2p_i;J_i=1,M_i=0\to J_f}-\sigma_{2p_i;J_i=1,M_i=1\to J_f}\right)\\&\times\cos(2\beta).\end{aligned} \tag{23}$$

The polarized cross sections in the space-fixed reference frame are obtained for particular values of β angle (see Ref. [4]):

$$\sigma^{(E)}_{2p_i;J_i=1\to 2p_f;J_f}(\beta=0)=\sigma_{2p_i;J_i=1,M_i=0\to 2p_f;J_f}, \tag{24}$$

$$\sigma^{(E)}_{2p_i;J_i=1\to 2p_f;J_f}\left(\beta=\frac{\pi}{2}\right)=\sigma_{2p_i;J_i=1,M_i=1\to 2p_f;J_f}. \tag{25}$$

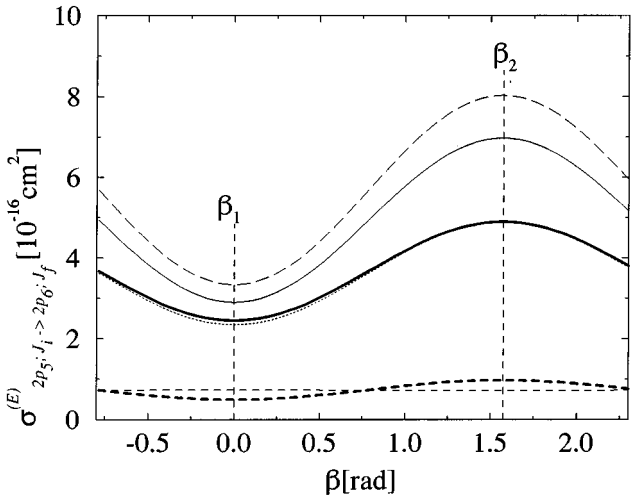

FIG. 9. Comparison between TE and SE experimental and theoretical results of the $\sigma^{(E)}_{2p_5;J_i=1\to 2p_6;J_f=1}$ cross section as a function of the β angle between the electric field vector **E** of the laser beam and the asymptotic relative velocity **g**. The experimental values were measured at collision energies $E=100$ meV (thick dashed line) and 450 meV (thick solid line). The calculations were performed at collision energies of 100 meV (thin dashed line), 350 meV (dotted line), 450 meV (thin solid line), and 525 meV (long dashed line). We indicate on the figure the limit angles $\beta_1=0$ and $\beta_2=\pi/2$ [see Eqs. (24) and (25), respectively, in text], for which polarized cross sections in space-fixed representation can be extracted.

In Figs. 9 and 10, we show a comparison between experimental and theoretical results for the variation of the cross sections as a function of β angle in two cases (arbitrarily chosen): the transitions $2p_5\to 2p_6$ and $2p_7\to 2p_5$. In the case of the SE range, the experimental data were measured

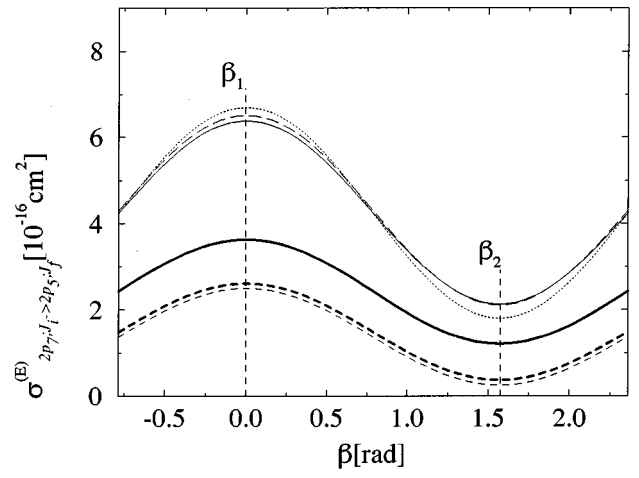

FIG. 10. Comparison between TE and SE experimental and theoretical results of the $\sigma^{(E)}_{2p_7;J_i=1\to 2p_5;J_f=1}$ cross section as a function of the angle β between the electric field vector **E** of the laser beam and the asymptotic relative velocity **g**. The experimental value was measured at collision energies $E=140$ meV (thick dashed line) and 500 meV (thick solid line). The calculations were performed at collision energies of 140 meV (thin dashed line), 350 meV (dotted line), 500 meV (thin solid line), and 525 meV (long dashed line). For the signification of β_1 and β_2 angles, see Fig. 9.

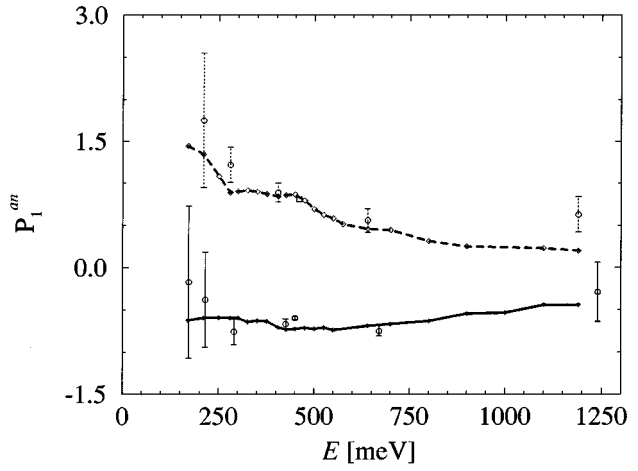

FIG. 11. Comparison between the SE experimental results [10] and our theoretical calculations of the energy dependence of the anisotropy parameter $P_1^{\rm an}$ [defined in Eq. (26) in text], for the transitions $2p_5\to 2p_6$ (solid line) and $2p_5\to 2p_7$ (dashed line). For experiments, only the statistical error bars [calculated with Eq. (27): see text] are indicated.

with an uncertainty in the determination of the collision energy (experiments referred to as ''non-energy-resolved'' in Ref. [10]). The error bar in the collision energy corresponds approximately to the range between the two energies for which we have done the calculations (at $E=350$ and 525 meV, respectively). Taking into account the systematic error bar, it is evident that in the TE range the agreement between theory and experiment is very good and that in the SE range our theoretical curve reproduces well the shape of the experimental curve. The same agreement is obtained for all the transitions for which experimental results are available.

The discussion about absolute cross sections in the SE range seem to indicate a possible calibration problem in the experiments of Boom *et al.* [9,10]. If our hypothesis is correct, it would be reasonable to look for parameters which depend upon cross-section ratios, because they do not depend upon calibration. So are the anisotropy parameters defined in Refs. [9,10], which provide information about the importance of the polarization effect for each of the analyzed transitions. For the cases presented above (where the initial states have an electronic momentum $J_i=1$), the polarization effect can be measured by the anisotropy parameter $\Pi_1^{\rm an}$ defined as

$$\prod_1^{\rm an}=P_1^{\rm an}=\frac{\sigma_{2p_i;J_i=1M_i=0\to 2p_f;J_f}-\sigma_{2p_i;J_i=1M_i=1\to 2p_f;J_f}}{\sigma_{2p_i;J_i=1\to 2p_f;J_f}}. \tag{26}$$

In Figs. 11 and 12, we display some examples of the energy variation, in the SE range, of the $P_1^{\rm an}$ parameter computed from our theoretical cross-sections values together with a few experimental results. We have chosen the transitions $2p_5\to 2p_6$, $2p_5\to 2p_7$, $2p_7\to 2p_4$, and $2p_7\to 2p_5$. For the experimental points, the statistical error bar is considered and evaluated with the formula

$$\delta P=\frac{\sigma_1}{\sigma^2}\,\delta\sigma_0+\frac{\sigma_0}{\sigma^2}\,\delta\sigma_1, \tag{27}$$

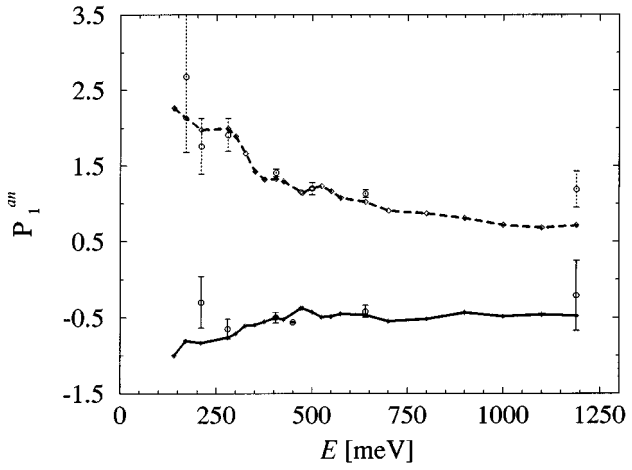

FIG. 12. Same as Fig. 11, but for the transitions $2p_7 \rightarrow 2p_4$ (solid line) and $2p_7 \rightarrow 2p_5$ (dashed line).

where

$$\sigma_0 \equiv \sigma_{2p_i;J_i=1M_i=0\rightarrow 2p_f;J_f},$$

$$\sigma_1 \equiv \sigma_{2p_i;J_i=1M_i=1\rightarrow 2p_f;J_f},$$

and

$$\sigma = (\sigma_0 + 2\sigma_1)/3;$$

$\delta\sigma_0$ and $\delta\sigma_1$ are the statistical error bars of the absolute polarized cross sections given in Refs. [9,10]. Our calculations are now in excellent agreement with the experimental results for all transitions in both energy ranges. Considering the behavior of the curves, we may note that the character of the polarization effect is reversed in the case of $2p_5 \rightarrow 2p_6$ and $2p_7 \rightarrow 2p_4$ transitions, as compared to $2p_5 \rightarrow 2p_7$ and $2p_7 \rightarrow 2p_5$ transitions. We find that with increasing collision energy the polarization effect tends to zero in all cases.

For transitions where the initial levels are $|2p_i;J_i=2,M_i\rangle$ and $|2p_i;J_i=3,M_i\rangle$, it was proved by experimental evidence that the experimental anisotropy parameters correspond to the theoretical parameters $\Pi_2^{an} = P_2^{an} - Q_2^{an}$ and $\Pi_3^{an} = P_3^{an} - 2.7Q_3^{an} + 1.8R_3^{an}$, respectively (see Ref. [10]), where P_J^{an} is easily deduced from Eq. (26), while the Q_j^{an} and R_J^{an} anisotropy parameters are given in [10]. We find that in the case when the initial level is $|2p_i;J_i=2,M_i\rangle$, the anisotropy parameter is given by the formula

$$\Pi_2^{an} = \frac{\sigma_{2p_i;J_i=2M_i=0\rightarrow 2p_f;J_f} - \sigma_{2p_i;J_i=2M_i=2\rightarrow 2p_f;J_f}}{4\sigma_{2p_i;J_i=2\rightarrow 2p_f;J_f}}, \tag{28}$$

and for an initial level $|2p_i;J_i=3,M_i\rangle$ it is

$$\Pi_3^{an} = \frac{-2.15\sigma_{2p_i,J_i=3M_i=0\rightarrow 2p_f;J_f} + 3.39\sigma_{2p_i;J_i=3M_i=1\rightarrow 2p_f;J_f} - 1.35\sigma_{2p_i;J_i=3M_i=2\rightarrow 2p_f;J_f} + 0.11\sigma_{2p_i;J_i=3M_i=3\rightarrow 2p_f;J_f}}{\sigma_{2p_i,J_i=3\rightarrow 2p_f;J_f}}. \tag{29}$$

We have calculated the anisotropy parameters through the formulas (28) and (29) using our polarized cross-section results. In Tables I and II we compare them to the experimental parameters and the theoretical values calculated by Boom *et al.* [10], for several transitions with initial levels $|2p_i;J_i=2,M_i\rangle$ and $|2p_i;J_i=3,M_i\rangle$, respectively. In most cases, we reproduce nicely the experimental results. With few exceptions, we are also in good agreement with the previous calculations, the small differences being attributed to the different choice in the description of the core-core interaction.

Finally, we summarize the comparison between our calculations and the results of absolute polarized cross section obtained in SE experiments [9] by considering the *mean* value of the ratio between the measured absolute cross sections:

$$K = \frac{\sigma^{expt}_{2p_i;J_iM_i\rightarrow 2p_f;J_f}}{\sigma^{calc}_{2p_i;J_iM_i\rightarrow 2p_f;J_f}}. \tag{30}$$

The K parameter is presented in Fig. 13, as an histogram, for *all* transitions for which we have performed calculations. We have considered all collision energies for which SE experimental results are available and also both types of detection methods (RC and SB). The histogram drawn with a solid line includes only statistical errors, while the dotted histogram corresponds to the ratio K moved up with the systematic error bar of 22%. If only statistical error is considered, we find that the *mean* value of K is about 0.63 for the set of transitions considered. With the systematic error included, this value became approximately 0.78. In the ideal case, the ratio K must be equal to 1. We can see on the histogram that even if we take into account all the error bars, the ratio K is less than 1.

Therefore, all comparisons considering either absolute cross sections or relative parameters derived from them lead us to the conclusion that the hypothesis of a calibration problem in the SE experiments should be considered seriously.

B. Discussion of the sensitivity of the dynamical calculations to the potentials

The discrepancy between the quantal calculations and the experimental results has been attributed by Boom *et al.* [9,10] to deficiencies in the long-range part of the model potential curves given in paper I. Indeed, when the collision

TABLE I. Comparison between the experimental anisotropy parameter and the equivalent theoretical one Π_2^{an}, which is computed through formula (28) for the case $J_i=2$, as shown in Ref. [10]. The experimental and previous theoretical results are taken from in Ref. [10].

Transitions	E [meV]	Π_{expt}^{an} Ref. [10]	E [meV]	Π_2^{an} Ref. [10]	Π_2^{an} Our work
$2p_4\rightarrow 2p_6$	430	−0.31	430		−0.080
			525	−0.07	−0.064
$\rightarrow 2p_7$	430	−0.10	430		−0.016
			525	−0.02	−0.036
$\rightarrow 2p_8$	430	0.37	430		0.263
			525	0.27	0.284
$\rightarrow 2p_9$	430	0.07	430		−0.028
			525	−0.04	−0.048
$2p_6\rightarrow 2p_4$	450	0.13	450		0.119
			525	0.13	0.089
$\rightarrow 2p_5$	450	−0.17	450		−0.137
			525	−0.18	−0.163
$\rightarrow 2p_7$	450	−0.04	450		−0.058
			525	−0.08	−0.092
$\rightarrow 2p_8$	450	0.23	450		0.249
			525	0.16	0.249
$\rightarrow 2p_9$	450	0.19	450		0.067
			525	0.04	0.066
$2p_8\rightarrow 2p_4$	490	0.34	490		0.412
			525	0.41	0.428
$\rightarrow 2p_5$	490	−0.06	490		−0.065
			525	−0.09	−0.079
$\rightarrow 2p_6$	490	0.14	490		0.378
			525	0.31	0.359
$\rightarrow 2p_7$	500	0.05	500		0.066
			525	0.07	0.046
$\rightarrow 2p_9$	500	−0.13	500		−0.085
			525	−0.08	−0.074
$\rightarrow 2p_{10}$	500	−0.15	500		−0.217
			525	−0.12	−0.223

energy increases, they found an enhancement of the contribution of large impact parameters in the cross sections. Significant contributions came from distances larger than the position R_{ij} of any avoided crossing between two adiabatic molecular curves i and j [9,10]. We have observed a similar effect in our calculations, and this is particularly obvious in transitions for which a single avoided crossing exists. As a relevant example, we focus on the $2p_7\rightarrow 2p_6$ transition, for which the energy splitting is small (194.38 meV) and there is only one avoided crossing between the adiabatic potentials curves for $\Omega=1$, at $R_{76}=7.4a_0$ (see Fig. 15). We display in Fig. 14 the partial polarized cross section $\sigma^P_{2p_7;J_iM_i\rightarrow 2p_6;J_f}$ for $M_i=1$, drawn as a function of the impact parameter $b=\sqrt{P(P+1)/2\mu E}$. It is clear that in the SE range, the cross section becomes dominated by the contribution of large impact parameters ($b>R_{76}$). The same effect is observed for the cross section $M_i=0$. This phenomenon, however, is not true for all transitions, and a more detailed discussion, in connection with a semiclassical model, will be presented in a forthcoming paper.

In order to check the sensitivity of the results to the value of the long-range potentials, we have modified the $\mathscr{V}_\sigma(R)$ potential in the region $R>9.75a_0$, beyond all existing avoided crossings. In this region the core-core interaction is described by the polarization term, and the $\mathscr{V}_\pi(R)$ potential is negligible, so that the only quantity which is questionable is the $\mathscr{V}_\sigma(R)$ potential. It can be fitted by an exponential function $\alpha\exp(-\beta R)$, with $\alpha=8.759\times10^5$ cm^{-1} and $\beta=0.813$ a.u. We have modified the $\mathscr{V}_\sigma(R)$ potential by keeping the continuity of the derivative at $R=9.75a_0$ and changing the asymptotic behavior considering two extreme cases with $\alpha=2.3\times10^9$ cm^{-1}, $\beta=1.614$ a.u. and $\alpha=3.0\times10^4$ cm^{-1}, $\beta=0.493$ a.u. The corresponding variation of the cross section is less than 10% in all cases except the $2p_5\rightarrow 2p_4$ transition, where it is at most 20%. In the latter case the avoided crossing is located at the largest internuclear distance $R_{54}=8.6a_0$. Moreover, we have verified that the TE cross sections are more sensitive to the long-range potentials than the cross section in the SE range: At 1200 meV, the cross sections are modified by less than 5%, except

TABLE II. Same as Table I for an initial state $J_i=3$. The theoretical anisotropy parameter is computed from formula (29).

Transitions	E [meV]	Π^{an}_{expt} Ref. [10]	E [meV]	Π^{an}_3 Ref. [10]	Π^{an}_3 Our work
$2p_9\rightarrow 2p_4$	450	0.150	450		0.212
			525	0.16	0.165
$\rightarrow 2p_5$	450	0.153	450		0.201
			525	0.24	0.257
$\rightarrow 2p_6$	450	0.100	450		0.136
			525	0.12	0.101
$\rightarrow 2p_7$	450	0.116	450		0.122
			525	0.13	0.116
$\rightarrow 2p_8$	450	0.009	450		−0.015
			525	−0.01	−0.029
$\rightarrow 2p_{10}$	450	0.065	450		0.093
			525	0.067	0.066

for the $2p_5\rightarrow 2p_4$ transition, where the modification reaches 18%. If the discrepancy between the calculations and the SE experimental data was due to to a defect in the long-range behavior of the potentials, we would also get discrepancy with the TE experimental data, which is not the case.

It should be noted that the interpretation of the collision mechanism by avoided crossings between two adiabatic potentials in the Hund's case *c* coupling scheme is certainly not valid at high collision energies, when the fine-structure splitting becomes much smaller than the collision energy. In the case discussed above ($2p_7\rightarrow 2p_6$ transition), the fine-structure splitting is *24 meV*, so that in the SE range when the energy becomes larger than 1 eV, a representation using Hund's case *e* curves should be more adapted, as discussed in Ref. [15]. A look at Fig. 15 where the typical collision energy is compared to the splitting between various curves shows that it is not realistic to isolate two adiabatic curves and that the diabatic representation discussed at the beginning of the paper is better adapted.

As the determination of the short-range potential is also questionable, we also have checked how our results would be modified in the extreme case of a hard wall at $3.5a_0$. The latter value was chosen according to our discussion for the validity of model potential calculations (see Sec. II). The cross sections were modified by less than 4%, except for a few cases where, due to the presence of an avoided crossing in the region $R<3.5a_0$, a variation of 15% is reached. We therefore cannot attribute the discrepancy with the SE ex-

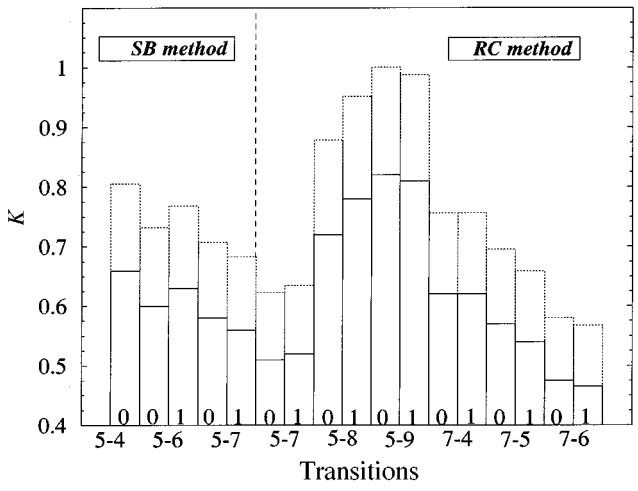

FIG. 13. *K* value [defined in Eq. (30)] considering both detection methods used in SE experiments [9] [single-burst (SB) and pseudorandom correlation (RC) time-of-flight methods] and the present calculations, for *all* transitions in which the initial state has $J_i=1$ and all collision energies for which experimental results are available. The dotted histogram corresponds to the case where for SE experiments the systematic error (of 22%: see in Ref. [10]) was considered. The transitions are indicated by the index of initial and final atomic states i and f, as i-f. The values of quantum number M_i are also indicated. Except for $2p_5\rightarrow 2p_4$ transition, for which the only $M_i=0$ case is shown, for all the others, both M_i values were considered.

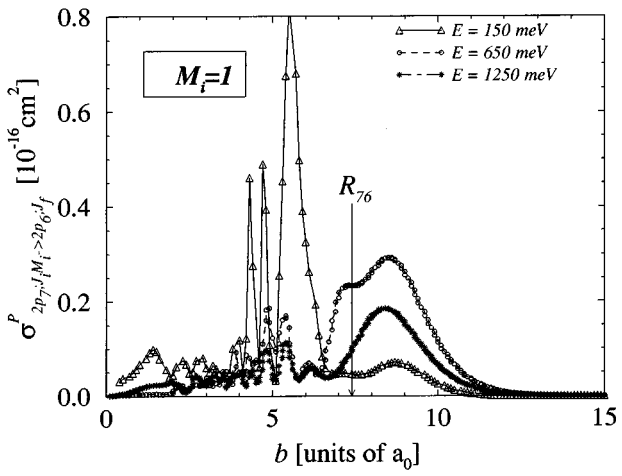

FIG. 14. Variation of the partial polarized cross section $\sigma^P_{2p_7;J_iM_i\rightarrow 2p_6;J_f}$ as a function of the impact parameter b at three collision energies: $E=150$ meV (triangles), 650 meV (circles), and 1250 meV (asterisks), for the test transition $2p_7\rightarrow 2p_6$, with $M_i=1$. The position of the avoided crossing ($R_{76}=7.4a_0$) for the relevant adiabatic potentials for $\Omega=1$ is shown.

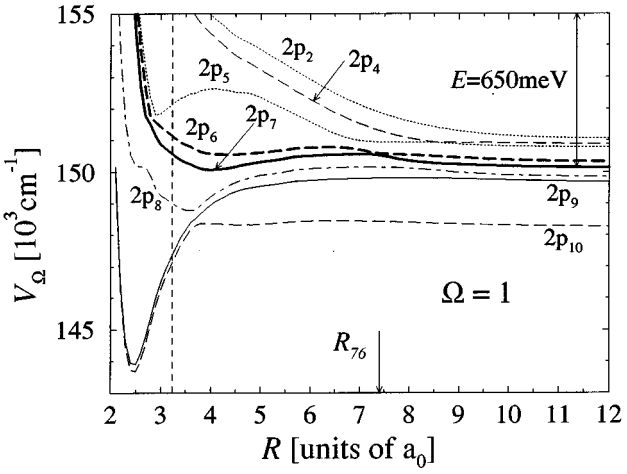

FIG. 15. Hund's case *c* adiabatic potential curves with $\Omega=1$. The order of magnitude of a collision energy typical of the SE experiments is indicated.

perimental data to our choice of the core-core term. Another check for the importance of the core-core term is provided by the comparison between our calculations and the previous quantal calculations of Refs. [6] and [10].

Finally, our tests show that the correct description of the potentials in the region $3.5a_0<R<5.6a_0$, where the core-core interaction is not yet dominated by the polarization term (see Sec. II), does play an important role and could modify the cross-section values up to 60%, justifying our effort to determine $\mathscr{W}_\sigma(R)$ and $\mathscr{W}_\pi(R)$ potentials with accuracy. Our present choice will be checked further in forthcoming calculations of the differential cross section.

V. CONCLUSION

We have performed quantal calculations for the absolute polarized cross sections and anisotropy parameters in the case of the intramultiplet transitions for $Ne^*(2p^5 3p) + He(^1S_0)$ collisions. The 36 coupled equations have been written in a diabatic representation, in which the interaction between the two atoms is determined from model potential calculations of Hennecart and Masnou-Seeuws [5], combined with short-range core-core potentials fitted on spectroscopic data for the $HeNe^+$ molecular ion. From the numerical solution of the equations, we have shown that one must be careful to extract the scattering **S** matrix by considering asymptotic wave functions which correspond to eigenvalues P of the total angular momentum; it is not justified to use the approximation $N\sim P$, where N is the eigenvalue of the angular momentum associated with the relative motion of the nuclei and differs from P only by a few units. This sensitivity is due to the rapid variation of the phase as a function of P, connected to large values of classical scattering angle. In the treatment of collisions in the presence of a magnetic field, necessary to interpret existing experiments at thermal energies [33], it will therefore not be possible to simplify equations using the convenient approximation $N\sim P$.

In the thermal collision energy range ($60\text{ meV}<E<150\text{ meV}$), the cross sections are in good agreement with the absolute data of Manders *et al.* [4,6]. They are not very sensitive to the position of the repulsive wall in the core-core term, so that our present model for the short-range potentials should be checked further by computing differential cross sections. However, they depend upon the representation of such term in the range $3.5a_0<R<5.6a_0$, justifying the need for *ab initio* calculations when more accurate investigations are considered.

At superthermal collision energies ($170\text{ meV}<E<1250\text{ meV}$), we have shown that for all transitions investigated, the energy variation of the computed polarized cross sections yields curves which have the same behavior as the experimental data of Boom *et al.* [9]. Analyzing the relative data, we have found good agreement between our theoretical results and the measurements of Refs. [9,10] for the anisotropy parameters. However, we confirm the 30–40 % discrepancy between theory and experimental absolute values. We have discussed the sensitivity of the results to the long-range part of the potentials and to the description of the core-core term, showing that this could not explain the discrepancy. We therefore suggest that a calibration systematic error in the experimental data should seriously be considered.

The oscillations in the cross sections, as a function of collision energy, due to interference effects, will be discussed in a forthcoming paper. We shall also present a semiclassical model to interpret the increasing contribution of large impact parameters for some transitions at superthermal energies, due to a new collision mechanism with long-range fine-structure decoupling. One important development of the present work will be the interpretation of collision experiments in the presence of a magnetic field.

[1] J. P. J. Driessen and S. R. Leone, J. Phys. Chem. **96**, 6136 (1992).
[2] H. C. W. Beijerinck, in *The Physics of Electronic and Atomic Collisions (XVI International Conference)*, edited by A. Dalgarno, R. S. Freund, P. M. Koch, M. S. Lubell, and T. B. Lucatorto, AIP Conf. Proc. No. 205 (AIP, New York, 1989), pp. 317–324.
[3] M. P. I. Manders, J. P. J. Driessen, H. C. W. Beijerinck, and B. J. Verhaar, Phys. Rev. Lett. **13**, 1577 (1986).
[4] M. P. I. Manders, J. P. J. Driessen, H. C. W. Beijerinck, and B. J. Verhaar, Phys. Rev. A **37**, 3237 (1988).
[5] D. Hennecart and F. Masnou-Seeuws, J. Phys. B **18**, 657 (1985).
[6] M. P. I. Manders, W. B. M. van Hoek, E. D. J. Vredenbregt, G. J. Sandker, H. C. W. Beijerinck, and B. J. Verhaar, Phys. Rev. A **39**, 4467 (1989).
[7] H. Kucal, D. Hennecart, and F. Masnou-Seeuws, Z. Phys. D **13**, 241 (1989).
[8] H. Kucal, D. Hennecart, and F. Masnou-Seeuws, Chem. Phys. **145**, 163 (1990).
[9] W. Boom, S. S. Op. de Beek, R. A. M. L. van Galen, F. J. J. Huijsmans, H. C. W. Beijerinck, and B. J. Verhaar, Phys. Rev. A **49**, 4660 (1994).
[10] W. Boom, R. A. M. L. van Galen, B. J. P. Klaver, S. S. Op. de Beek, J. T. A. Heier, H. C. W. Beijerinck, and B. J. Verhaar, Phys. Rev. A **51**, 3837 (1995).

[11] S. Feneuille, M. Klapisch, E. Koenig, and S. Liberman, Physica (Utrecht) **48**, 571 (1970).
[12] M. Aymar (private communication).
[13] P. Valiron, R. Gayet, R. McCarroll, F. Masnou-Seeuws, and M. Philippe, J. Phys. B **12**, 53 (1979).
[14] H. Margenau, Phys. Rev. **56**, 1000 (1939).
[15] E. E. Nikitin and S. Ya. Umanskii, *Theory of Slow Atomic Collisions* (Springer-Verlag, Berlin, 1984).
[16] A. Dalgarno and A. E. Kingston, Proc. R. Soc. London, Ser. A **245**, 424 (1960).
[17] L. Ya. Efremenkova, A. A. Radsig, and B. M. Smirnov, Opt. Spectrosc. **36**, 35 (1974).
[18] I. Dabrowski and G. J. Herzberg, Mol. Spectrosc. **73**, 183 (1978).
[19] P. E. Siska, J. Chem. Phys. **73**, 2372 (1980).
[20] R. H. G. Reid, J. Phys. B **6**, 2018 (1973).
[21] F. H. Mies, Phys. Rev. A **7**, 942 (1973).
[22] J-M. Launay and E. J. Roueff, J. Phys. B **10**, 879 (1977).
[23] A. P. Hickman, D. L. Huestis, and R. P. Saxon, J. Chem. Phys. **98**, 5419 (1993).
[24] B. Zygelman, A. Dalgarno, and R. D. Sharma, Phys. Rev. A **49**, 2587 (1994).
[25] B. Pouilly and M. H. Alexander, J. Chem. Phys. **86**, 4790 (1987).
[26] B. Pouilly, B. J. M. Robbe, and M. H. Alexander, J. Chem. Phys. **91**, 1658 (1989).
[27] M. H. Alexander and B. Pouilly, J. Chem. Phys. **90**, 5373 (1989).
[28] D. A. Varshalovich, A. N. Moskalev, and V. K. Khersonskii, *Quantum Theory of Angular Momentum* (World Scientific, Singapore, 1989).
[29] B. R. Johnson, J. Comput. Phys. **13**, 445 (1973).
[30] P. Valiron, thèse d'état, Université de Bordeaux I, 1976 (unpublished).
[31] M. P. I. Manders, W. M. Ruyten, F. v. d. Beucken, J. P. J. Driessen, W. J. T. Veugelers, P. H. Kramer, E. J. D. Vredenbregt, W. B. M. van Hoek, G. J. Sandker, H. C. W. Beijerinck, and B. J. Verhaar, J. Chem. Phys. **89**, 4777 (1988).
[32] C. Bahrim, Ph.D. thesis, Orsay, 1997 (unpublished).
[33] S. Matsumoto, Y. Ishitani, A. Hirabayashi, and T. Fujimoto, Phys. Rev. A **44**, 4316 (1991).